

Hydraulic model calibration using CryoSat-2 observations in the Zambezi catchment

Cécile M. M. Kittel¹, Simbidzayi Hatchard², Jeffrey C. Neal², Karina Nielsen³, Paul D. Bates², Peter Bauer-Gottwein¹

¹Department of Environmental Engineering, Technical University of Denmark, Kgs. Lyngby, Denmark

²School of Geography, University of Bristol, Bristol, United Kingdom

³National Space Institute, Technical University of Denmark, Kgs. Lyngby, Denmark

Corresponding author: Cécile M. M. Kittel (ceki@env.dtu.dk)

Key Points:

- We use satellite altimetry observations from CryoSat-2 and a steady-state solver to calibrate hydraulic model parameters
- We develop an outlier filtering method for CryoSat-2 observations in ungauged catchments based on rainfall-runoff model simulations
- We integrate the altimetry observations in an efficient global calibration approach at low cost compared to a 1D hydrodynamic model

Abstract

Geodetic altimeters provide unique observations of the river surface longitudinal profile due to their long repeat periods and densely spaced ground tracks. This information is valuable for calibrating hydraulic model parameters, and thus for producing reliable simulations of water level for flood forecasting and river management, particularly in poorly instrumented catchments. In this study, we present an efficient calibration approach for hydraulic models based on a steady-state hydraulic solver and CryoSat-2 observations. In order to ensure that only coherent forcing/observation pairs are considered in the calibration, we first propose an outlier filtering approach for CryoSat-2 observations in data-scarce regions using simulated runoff produced by a hydrologic model. In the hydraulic calibration, a steady-state solver computes the WSE profile along the river for selected discharges corresponding to the days of CryoSat-2 overpass. In synthetic calibration experiments, the global search algorithm generally recovers the true parameter values in portions of the river where observations are available, illustrating the benefit of dense spatial sampling from geodetic altimetry. The most sensitive parameters are the bed elevations. In calibration experiments with real CryoSat-2 data, validation performance against both Sentinel-3 WSE and in-situ records is similar to previous studies, with RMSD ranging from 0.43 to 1.14 m against Sentinel-3 and 0.60 to 0.73 against in-situ WSE observations. Performance remains similar when transferring parameters to a one-dimensional hydrodynamic model. Because the approach is computationally efficient, model parameters can be inverted at high spatial resolution to fully exploit the information contained in geodetic CryoSat-2 altimetry.

1. Introduction

Climate change and human activities have altered river regimes globally, posing significant challenges for water resources managers (Mahé et al., 2013). Flood and drought patterns are changing calling for robust flood hazard and risk assessment. Many river basins are currently ungauged or sparsely gauged (Hannah et al., 2011), as monitoring efforts and data accessibility have severely declined in recent decades (Vörösmarty et al., 2001). However, a reasonable hydraulic representation of river channels is key to producing meaningful large-scale flood models and typically relies on ground monitoring. Simulating river hydraulics at large scale in poorly instrumented regions requires adapted model structures and simplifications to compensate for constraints on computational resources and insufficient ground observations.

Remote sensing observations can be used to retrieve hydraulic parameters and have become a key supplement to in-situ observations in hydrological studies. When parameters cannot be sensed even remotely, calibration is an important step to ensure that the simulated quantities agree with observations of the system (Michailovsky et al., 2012). Very often, bathymetry and channel roughness need to be estimated through calibration or assumptions made by the modeler, e.g. regarding channel geometry (Alsdorf et al., 2007). Effective estimation methods in data-poor regions are needed.

Satellite radar altimeters can measure the water surface elevation (WSE) of inland water bodies, which can be used as an alternative to in-situ level observations. WSE from satellite radar altimetry has been used increasingly in hydrodynamic model calibration studies as a supplement to in-situ gauge data (Paiva et al., 2013; Schneider, Tarpanelli, et al., 2018) or even as a possible surrogate in ungauged basins (Getirana et al., 2013; Jiang et al., 2019; Liu et al., 2015). Dense water level profiles have been proven useful in the estimation of distributed hydraulic parameters (F. O’Loughlin et al., 2013; Paris et al., 2016; Schumann et al., 2010). To capture the small-scale variability of river morphology, the spatial sampling must be denser than what can be achieved with short-repeat missions (down to 52 km at the Equator for the two Sentinel-3 satellites). In that respect, geodetic altimeters such as CryoSat-2 provide the opportunity to extract longitudinal profiles of rivers.

Although not designed for hydrological applications, the benefit of high spatial sampling density of geodetic missions for hydraulic studies has been proven in recent years (Jiang et al., 2019; Schneider, Ridler, et al., 2018; Schneider, Tarpanelli, et al., 2018; Tourian et al., 2016). Schneider et al. (2018) exploited the dense spatial sampling of CryoSat-2 to calibrate channel roughness in the well-gauged Po River at a finer spatial resolution. They compared

homogenous roughness parameters to spatially distributed parameters with increasing the spatial resolution from subreach level to 10 km-long sections. The RMSE (Root Mean Square Error) against in-situ observations improved by up to 29 cm. They showed a strong correlation between the channel sinuosity and the spatially variable calibrated channel roughness. Jiang et al. (2019) showed that missions with high spatial coverage, such as CryoSat-2, improved the RMSE against ground observations by up to 4 cm compared to missions with wider ground track spacing (i.e. the spacing between satellite tracks) such as Envisat or Jason-2 and 3. Furthermore, the sharpness of the parameter estimates increased with decreasing ground-track spacing and increasing spatial detail. Tourian et al. (2016) reached a similar conclusion in a study on spatiotemporal densification of altimetry over rivers. The quality of time series at virtual stations deteriorated slightly when including CryoSat-2 data due to assumptions pertaining to the spatial interpolation. However, CryoSat-2 decreased the bias by increasing the spatial representation of the river profile.

An important step in using satellite altimetry for inland water applications is outlier filtering. Typically, outliers are removed using secondary datasets such as a Digital Elevation Model (DEM) or binary water/land masks (Jiang et al., 2017; Schneider et al., 2017; Schwatke et al., 2015) or by evaluating the observations themselves, e.g. the return waveforms or the backscatter coefficients (e.g. Boergens et al., 2017; Dinardo et al., 2018; Schwatke et al., 2015; Zhang et al., 2020). For larger water bodies or short return missions, statistical outlier removal can be used to further refine the filtering (e.g. Nielsen et al., 2015; Schwatke et al., 2015; Zhang et al., 2020). For medium-sized rivers, the number of observations per ground track may be too low to perform meaningful statistical outlier removal. When bathymetry is unknown, WSE is dominated by the unknown bed elevation and errors larger than 1 m may be difficult to detect. This poses a challenge particularly for geodetic missions such as CryoSat-2, where the seasonal signal cannot be removed due to the long revisit time. The dense spatial sampling pattern is impractical for on-ground validation and comparison to traditional gauging stations would require aggregation of the observations at the expense of the valuable spatial resolution to obtain time series. Therefore, robust outlier removal procedures are needed to extract useful observations from geodetic altimetry datasets.

Water levels alone can only provide limited information, and the modelling and calibration problems must be adequately formulated to reflect the available observations. Getirana et al. (2013) and Liu et al. (2015) achieve good simulation results when calibrating channel roughness and bed elevation parameters simultaneously in spite of model equifinality. Jiang et al. (2019) investigated the information contained in altimetry WSE and the capability to recover parameter values (bed elevation, channel roughness and channel geometry) through calibration. Only the bed elevation could be consistently retrieved in combination with one of the other parameters. To avoid ambiguity, channel geometry can be inferred e.g. by assuming rectangular river cross-sections (Biancamaria et al., 2009; Jiang et al., 2019) or power channel shapes (Neal et al., 2015) and information from satellite imagery and global databases.

The inverse problem to determine hydrodynamic model parameters is highly non-linear and non-convex. Studies have used local iterative search algorithms such as Levenberg-Marquardt (Jiang et al., 2019; Schneider, Tarpanelli, et al., 2018) or global search algorithms (Getirana et al., 2013; Liu et al., 2015) to identify the optimal parameters. Global search algorithms are less sensitive to the starting point for non-convex problems; however, a higher number of simulations are usually required to search the parameter space adequately. The computational requirements to calibrate spatially distributed hydraulic parameters increase with the number of estimated parameters. Furthermore, solving the shallow water equations – even with efficient solvers – still requires long simulation time, including warm-up periods (Neal et al., 2012). Using a hydrodynamic solver in the inverse problem combined with a global search algorithm is infeasible due to resource requirements. Therefore, efficient calibration approaches balancing parameter accuracy and resources requirements are greatly needed.

In this study, we evaluate the combination of a steady-state solver of the shallow water equations and a global search algorithm for efficient calibration of hydraulic parameters against robustly selected CryoSat-2 observations.

Specifically, we

- Propose an outlier filtering method for CryoSat-2 observations suited for data-scarce regions based on runoff simulations
- Evaluate the capability of retrieving spatially distributed parameter values (i.e., channel roughness and bed elevation at least every 20 km) using a steady-state solution of the Saint-Venant equations and CryoSat-2 sampling pattern in synthetic calibration experiments
- Evaluate the method using real-world CryoSat-2 observations
- Assess the performance of the calibrated parameters in dynamic state using a hydrodynamic solver

The proposed method is most valuable in ungauged catchments, where observations of the targeted calibrated parameters are unavailable. Synthetic experiments allow us to evaluate how the calibration performs and to identify

potential limitations (e.g., parameter interactions, behavioral parameters). The full workflow is then assessed for tributaries of the Zambezi, by comparing Sentinel-3 water level and in-situ gauge data with the water levels simulated using a 1D hydrodynamic model parameterized with the calibrated parameters.

2. Study area

The Zambezi is located in Southern Africa and is the fourth largest river in Africa. It is 2,574 km long and drains a 1.4 million km² basin. Precipitation follows a declining North-to-South gradient, with an average of 1,500 mm in the North and 500 mm in the South. The wet season is between October and March. Flow is driven largely by the precipitation climatology but also by retention in large swamps and floodplains, and artificial reservoirs in the basin. The Zambezi provides key ecosystem services, supporting large populations of fauna and flora, but is also an important resource for the people living in the basin. We select three regions within the Zambezi as study areas: the Kafue, the Luangwa and the Upper Zambezi, upstream of the Barotse floodplain, specifically the tributaries Kabompo and Lungwebungo (**Figure 1**).

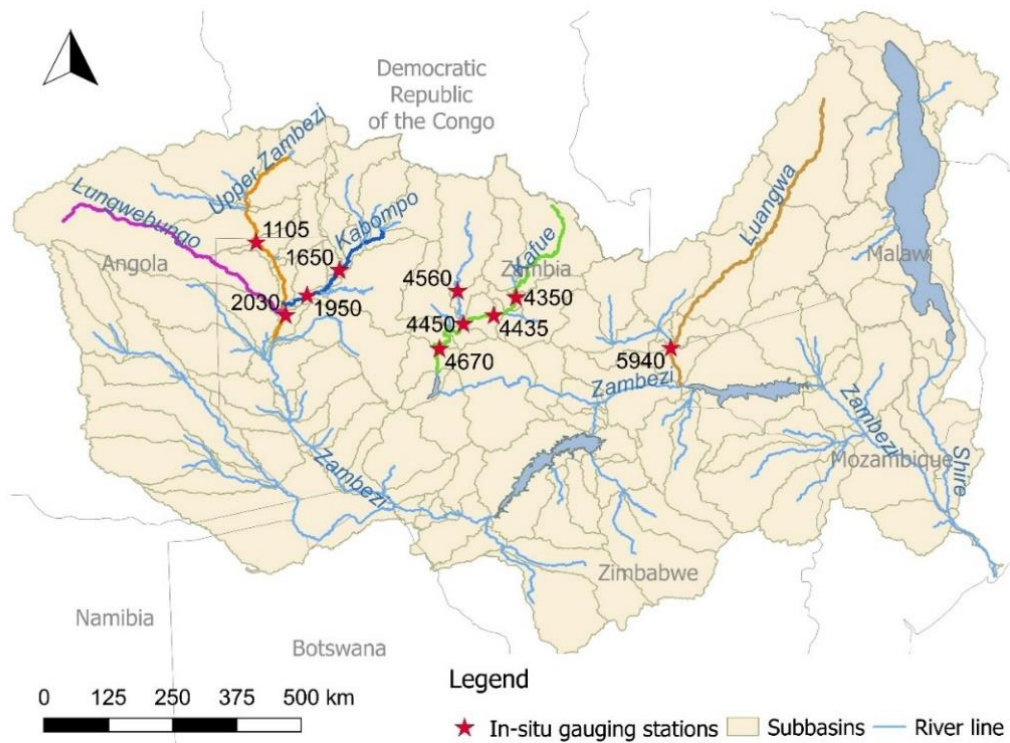


Figure 1 Study area and in-situ gauging stations. Calibration is performed for the five highlighted reaches (Lungwebungo, Kabompo, Upper Zambezi, Kafue and Luangwa).

3. Data

3.1. Radar Altimetry

3.1.1. CryoSat-2

CryoSat-2 Level 2 data were provided by the National Space Institute, Technical University of Denmark (DTU Space) for the period 16-07-2010 to 21-03-2018. The data is based on the 20Hz Level-1b ESA dataset and has been retracked at DTU Space using an empirical retracker based on a sub-waveform threshold (Villadsen et al., 2016). In

the Zambezi, CryoSat-2 operates only in Low Resolution Mode (LRM). The DEM and CryoSat-2 observations are reprojected onto the EGM2008 using VDatum (Myers et al., 2007).

3.1.2. Sentinel-3

The Sentinel-3 dataset is independent of the data used to calibrate the steady-state model and its virtual stations' monitoring network is denser and with more recent observations than the ground network. Sentinel-3 Level-2 WSE observations were obtained from the ESA GPOD (Grid Processing on Demand SAR Versatile Altimetric Toolkit for Ocean Research and Exploitation) service (available on <https://gpod.eo.esa.int/>). The data has been described and evaluated in Kittel et al. (2020b). Performance was quantified in the Upper Zambezi with RMSD varying between 2.9 and 31.3 cm. In the rest of the river catchment, there was good coherence between historical seasonal trends and the Sentinel-3 water surface elevation.

3.2. In-situ observations

In situ observations were available for five subcatchments in the Upper Zambezi and in the Kafue, and two out of 12 subcatchments in the Luangwa (Table S1 and Figure S1). The Zambezi River Authority (ZRA) kindly provided in-situ observations in the Upper Zambezi, completing the dataset from Michailovsky & Bauer-Gottwein (2014). In-situ discharge was used for the calibration of the rainfall-runoff model, while in-situ stage at two stations (Kabompo and Chavuma) was used to validate the hydraulic model. To avoid bias related to the vertical datum of the datasets, all records are referenced to their long-term mean and only amplitudes are compared.

3.1. Ancillary datasets

The river network is delineated using TauDEM v. 5 (Tarboton, 2015) and the MERIT DEM (Multi-Error-Removed Improved-Terrain Digital Elevation Model, Yamakazi et al., 2017). The model is forced using remote sensing observations: GPM (Global Precipitation Model) precipitation (Huffman et al., 2014) and ECMWF ERA-Interim (European Centre for Medium range Weather Forecasts - Interim Reanalysis) (Berrisford et al., 2011) temperature observations for the period 2001 to August 2019.

4. Methods

The entire workflow starting from data selection and ending with hydrodynamic simulation of water levels is shown in **Figure 2**. The methodology uses remote sensing inputs and two different models: a rainfall-runoff model and a hydraulic model in steady-state and dynamic mode.

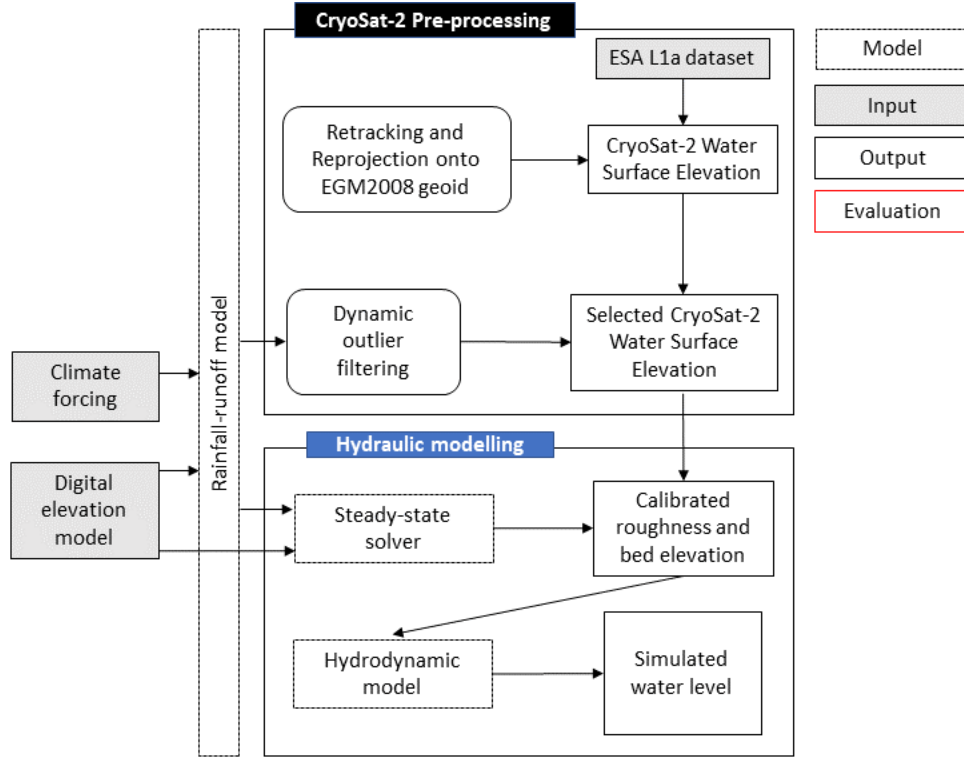


Figure 2 Schematic diagram presenting an overview of the main inputs, models and outputs of the calibration workflow presented in this study

4.1. CryoSat-2 pre-processing

First, we use the water occurrence maps from Pekel et al., (2016) to extract observations over the river. We use a threshold of 10% water occurrence frequency, and allow a 90-m buffer zone around the river mask based on the results from Schneider et al., (2018). The footprint in LRM is several km wide (2.5 km² with a diameter of 1.64 km) and a return signal from the water surface can be captured before and after the satellite has crossed the river. Parabolic distortions of the water levels due to this so-called “hooking effect” (Frappart et al., 2006; Maillard et al., 2015), are expected to be negligible at the scale of the buffer applied.

Second, we remove observations deviating from the local value of the MERIT DEM by more than 30 m. This ensures that the surface elevation is indeed within the 60 m satellite reception window. In total, CryoSat-2 crossed the Zambezi basin 3,724 times during the observation period, resulting in 291,287 observations over water bodies in the basin. Of those, 38,697 observations are over the river network itself. The rejection rate in step one is 10.5%, yielding 34,647 observations after this step.

Unlike previous studies, the third step takes into account the river dynamics by using the output of the rainfall-runoff model. We fit a one-dimensional smoothing spline in the space domain to the CryoSat-2 observations on each river reach. The spline curve is assumed to represent the mean water level for the days of observation. The expected deviation, Δy , from the mean level, y_{mean} , associated with the simulated discharge, Q , at the time of sensing assuming uniform flow and a wide rectangular channel is estimated using Manning’s equation for a wide rectangular channel

$$Q = \frac{1}{n} \sqrt{S} y^{\frac{5}{3}} \quad (1)$$

Q is the river discharge (m³/s) S is the bed slope (m/m), n is the channel roughness and y is the channel depth. Eq. 1 can be written for the mean discharge and water level and for the specific conditions on the day of CryoSat-2 overpass. By taking the log-transform and subtracting the two, we can isolate the Δy

$$\log(Q) - \log(Q_{mean}) = \frac{5}{3} (\log(y) - \log(y_{mean})) \quad (2)$$

$$\log(y) - \log(y_{mean}) = \log\left(\frac{y_{mean} + \Delta y}{y_{mean}}\right) = \frac{3}{5} \log\left(\frac{Q}{Q_{mean}}\right) \quad (3)$$

$$\Delta y = \left(\left(\frac{Q}{Q_{mean}} \right)^{\frac{3}{5}} - 1 \right) y_{mean} \quad (4)$$

We calculate the mean discharge, Q_{mean} , using only the days with CryoSat-2 observations. We use error propagation to estimate the total uncertainty of Δy based on assumed uncertainties of the discharge estimate, width, slope and Manning's number (**Table 1**). The effect of the spline function smoothing factor on the magnitude of the level deviation from the mean is mitigated by using an ensemble of spline curves using varying smoothing factors (0.01-4 times the number of observations in the reach). From the ensemble, we obtain different estimates of the deviation from the mean water level (Δy) for each CryoSat-2 observation. If the deviation falls outside of the predicted confidence interval of Δy for all smoothing factors the observation is rejected.

Table 1 Assumed uncertainties of parameters used to estimate the confidence interval of the WSE deviation Δy

Parameter	Estimate	Error propagation
Q	Daily discharge from rainfall-runoff model	+/- 25 %
Slope	From univariate spline function (minimum fixed at 10^{-5})	2 x standard deviation over the reach
Manning's n	0.035	Calibration range: 0.02-0.05
Width	GRWD database	+/- 25 %

4.2. Hydraulic model

4.2.1. Steady-state solver

The steady-state solver is based on the Saint-Venant equations, which express the mass balance and momentum balance equations for gradually varied one-dimensional flow in an open channel. The equations for the steady-state solver are detailed in the supporting information text, S1.

Equation 4 is the general form of the equation to solve, when assuming steady flow (i.e., constant discharge over time) and lateral inflow in a rectangular channel, where RHS (Right Hand Side) is the collection of terms not containing the derivative of the depth with respect to the chainage

$$\frac{dh}{dx} = \frac{\left(\frac{Q^2}{gA^3} \frac{\partial A}{\partial x} + S_0 - \frac{Q^2}{K^2} + \frac{2Q \times q}{gA^2} \right)}{\left(1 - \frac{Q^2}{gA^3} \frac{\partial A}{\partial h} \right)}$$

$$\frac{dh}{dx} = RHS(x, h(x)) \quad (4)$$

Where q is the lateral inflow at chainage x . Lateral inflow consists of runoff generated by the rainfall-runoff model in tributary subcatchments, which enters the hydrodynamic model at the most upstream node, and runoff produced in the subcatchment itself, which is distributed along the chainage proportionally to the contributing area.

The solver is initialized by calculating the downstream water level boundary condition using Manning's equation and a downstream slope of $2e^{-4}$ m/m at chainage, i . The downstream slope condition was chosen based on the average slope in the catchment and only affects the most downstream cross-section. The level is then calculated stepwise at Δx spatial increments, moving upstream along the channel and solving Eq. 4 either implicitly (Eq. 5) or explicitly (Eq. 6):

$$h_{i-1} = h_i - \frac{1}{2} \times (RHS(x_i, h_i) + RHS(x_{i-1}, h_{i-1})) \times \Delta x \quad (5)$$

$$h_{i-1} = h_i - RHS(x_i, h_i) \times \Delta x \quad (6)$$

The explicit solution is faster but requires smaller steps Δx to be stable, while the implicit solution is less sensitive to the spatial increments but requires the solution of a non-linear implicit equation for h_{i-1} at each time step. We tested the speed of the two solvers using a hypothetical formulation of the Kabompo reach channel. The solutions are virtually identical when solving the equations for steps of less than 500 m. The implicit solver runs in 5.3 seconds, whereas the explicit solution needs 0.06 seconds. Even when applying the implicit solution only to cross-sections with observations, the fastest computational time remains slower (0.17 seconds), and the large spatial increments affect the final solution. We therefore use the explicit solver using 250 m spatial steps. If the solution becomes numerically unstable, the spatial step is subdivided into 1 m increments.

We define calibration cross-sections every 20 km and at each CryoSat-2 observation. Although the steady-state solver is less computationally demanding than a full hydrodynamic calibration, the number of model parameters must still be constrained. Because of the CryoSat-2 orbit configuration, some observations and thus cross-sections are very closely spaced. This increases the number of calibration parameters and the risk of parameter correlation. We therefore remove cross-sections less than 5 km apart for shorter reaches (Kabompo and Upper Zambezi) and 10 km apart for longer reaches (Lungwebungo, Kafue and Luangwa).

4.2.2. Hydrodynamic model

LISFLOOD-FP is a coupled 1D/2D hydrodynamic model simulating the propagation of flood waves along channels (in 1D) and over floodplains (in 2D). LISFLOOD-FP has three solvers available for calculating channel flow. The kinematic wave routing model only considers the friction slope, assuming that local and convective acceleration terms are negligible and that the free surface gradient is equal to the bed slope. The diffusive wave model includes an additional pressure term. The sub-grid channel solves the full shallow water equations with the exception of the convective acceleration term (J. Neal et al., 2012). All three formulations are numerically stable (De Almeida et al., 2012). The model is specifically designed for poorly gauged catchments and has been implemented for a number of sites including the Niger River (J. Neal et al., 2012), the Congo (F. E. O'Loughlin et al., 2020), and rivers in the UK (Sosa et al., 2020).

We use LISFLOOD-FP to simulate the channel hydrodynamics in the transient state. The model requires information about channel geometry in the form of channel slope, channel width and bankfull depth from a DEM or surveyed cross-sections. The bank elevation is derived from the MERIT DEM, the width from the GRWD database and the bed elevation and channel roughness from the calibrated steady-state solver. The bankfull depth is the difference between the bed and bank elevations. The resolution of the input files is 900 m instead of the 250 m used by the steady-state solver to ensure reasonable computation time. The model is forced with daily discharge from headwater catchments and lateral inflow, both simulated by the rainfall-runoff model. Runoff increments are distributed according to the contributing area to each channel pixel, obtained from the river delineation. The model is run in 1D as a means to compare the steady-state solver to a transient solver by burning in the channel bed elevation into the DEM.

4.3. Hydrologic model

The CryoSat-2 pre-processing and the hydraulic model require runoff estimates. In ungauged catchments, these can be obtained using a hydrologic model. In this study we use a conceptual rainfall-runoff model of the Zambezi basin. The rainfall-runoff model is described in Kittel et al. (2018) and is based on the work by Zhang et al. (2008) who extended the Budyko framework's concept of limits to monthly and daily time steps. The model builds on a representation of the water balance through demand and supply at various levels. At each time step, Fu's representation of the Budyko curve (L. Zhang et al., 2008) is used to partition precipitation into catchment retention and runoff, and catchment retention into evapotranspiration, groundwater recharge and root-zone storage. The model is coupled to a Nash cascade of linear reservoirs simulating tributary processes.

The model is calibrated against in-situ discharge records from 1990-present after careful analysis to ensure hydrometeorological stationarity can be assumed between the observation and simulation periods. In order to parametrize ungauged subcatchments, we use the same catchment characteristics as proposed in Kittel et al. (2020): the subcatchments were grouped into calibration clusters using the European Space Agency Climate Change Initiative Land Cover map v.2 (ESA, 2017) and the MERIT DEM and calibrated holistically using an aggregated objective function at catchment scale allowing trade-offs between parameters in nested subcatchments. The regionalization and resulting calibration zones are summarized in Table S2. Performance was then evaluated based on the flow duration curves using equal flow volume classes as described in Westerberg et al. (2011) and on the daily discharge climatology Root Mean Square Deviation (RMSD). Additionally we use the Kling-Gupta Efficiency

to quantify post-calibration performance (Gupta et al., 2009). The model setup and performance are summarized in the supporting information, in Tables S1 and S2.

4.4. Hydraulic model calibration

4.4.1. Global search algorithm and performance statistics

The bed elevation and channel roughness are calibrated for each cross-section using the Shuffled Complex Evolution algorithm from the University of Arizona (SCEUA) developed by Duan et al., (1992) and implemented in Python using SPOTPY (Houska et al., 2015). The algorithm uses “complexes” to sample the parameter space. The complexes are groups of parameter samples, which are evolved independently and shuffled after each evolution cycle to ensure an efficient global search. The bed elevation parameters are initialized using a spline function interpolating between the CryoSat-2 WSE observations minus one meter to adjust for the water level. The bed elevation can vary between -5 m and 3 m from this initial value. The channel roughness is initialized at 0.04 and allowed to vary between 0.018 and 0.055. The calibration objective function consists of a data misfit term comparing the residuals between the CryoSat-2 WSE and the simulated WSE

$$E_i = (w_i + z_i) - WSE_{C2,i} \quad (7)$$

and a smoothness preference for the two parameters along the chainage

$$Sm_i = \frac{\sqrt{(p_i - p_{i-1})^2}}{f_{smooth}} \quad (8)$$

f_{smooth} is the smoothness preference: smaller values will give higher weight to Sm and force the solver to move towards a smoother solution with less abrupt changes in bed elevation or channel roughness, represented by p in Eq. 8. The calibration objective is

$$Obj = \sqrt{\frac{1}{2N} \left(\sum_{i=1}^N E_i^2 + \sum_{i=1}^N Sm_i^2 \right)} \quad (9)$$

The smoothness preference must be chosen to balance a realistic water surface and allowing features from the bed and channel roughness to be simulated. The preference is set to 1, giving equal weight to the smoothness and error objectives due to the types of parameters evaluated. Thus, the difference in magnitude between the objectives are balanced while still prioritizing a good fit between data and observation.

We compute three additional diagnostic performance measures to evaluate the post-calibration performance of the hydraulic model: the Pearson correlation coefficient, Spearman’s rank correlation coefficient and the non-parametric Kling-Gupta Efficiency (Pool et al., 2018). The Kling-Gupta Efficiency (KGE) combines the Pearson correlation coefficient, and the biases between mean and observed mean discharge and between the simulated and observed standard deviation. In the non-parametric version, the rank correlation is used instead, and the discharge variability performance is computed using the flow duration curve. This method is less sensitive to assumptions of data linearity, data normality and outliers (Pool et al., 2018).

4.4.2. Synthetic experiments

Synthetic calibration experiments are used to evaluate the capabilities of the steady-state solver and calibration algorithm to retrieve the bed elevation and channel roughness using CryoSat-2-type observations of WSE. We generate a synthetic set of parameters (i.e., bed elevation and Manning’s n at all cross-sections) to produce synthetic CryoSat-2 observations in the Kabompo reach, i.e., a synthetic representation of the true WSE. To reflect data uncertainties, the synthetic truth is perturbed with normally distributed random noise with varying standard deviations. The resulting three experiments are:

- 3 cm standard deviation representing in-situ water level accuracy
- 20 cm standard deviation representing high accuracy for altimetry WSE

- 40 cm standard deviation representing average accuracy for altimetry WSE

Parameter sensitivity is evaluated by conducting an extended Fourier amplitude sensitivity test (FAST) (Saltelli et al., 1999) as implemented in SPOTPY (Houska et al., 2015). We compare the total sensitivity of the bed elevation and channel roughness at each cross-section to assess the spatial sensitivity of the two parameters along the river chainage. Over 686,000 model runs are performed to achieve the recommended sampling of the parameter space based on the number of calibration parameters in the synthetic example (Houska et al., 2015; Saltelli et al., 1999).

4.4.3. Calibration against real-world observations

We then use the real-world CryoSat-2 observations and calibrate the bed elevation and channel roughness in five reaches in the Zambezi catchment. To ensure that the steady-state assumption is reasonable, we choose CryoSat-2 observations where the 10-day discharge gradient is less than 5% of the mean discharge. This is the case for 69.9% of the CryoSat-2 observations. To minimize the impact of uncertainties related to the CryoSat-2 observations and runoff simulations, we classify the simulated runoff and CryoSat-2 observations into discharge classes based on the runoff histogram and time of observation. The steady-state model is run for each class and residuals are calculated for all CryoSat-2 observations within the class.

5. Results

5.1. CryoSat-2 outliers filtering

Figure 3 illustrates the CryoSat-2 river longitudinal profiles and outlier filtering for each of the five reaches. In the downstream part of the Upper Zambezi, water level increases of 5 m are unlikely during the low flow season; therefore, the associated CryoSat-2 observations are rejected, however a similar increase may occur during the high flow season, highlighting the benefit of a dynamic threshold. The rejection rate is between 10% for Lungwebungo and 24% for Luangwa.

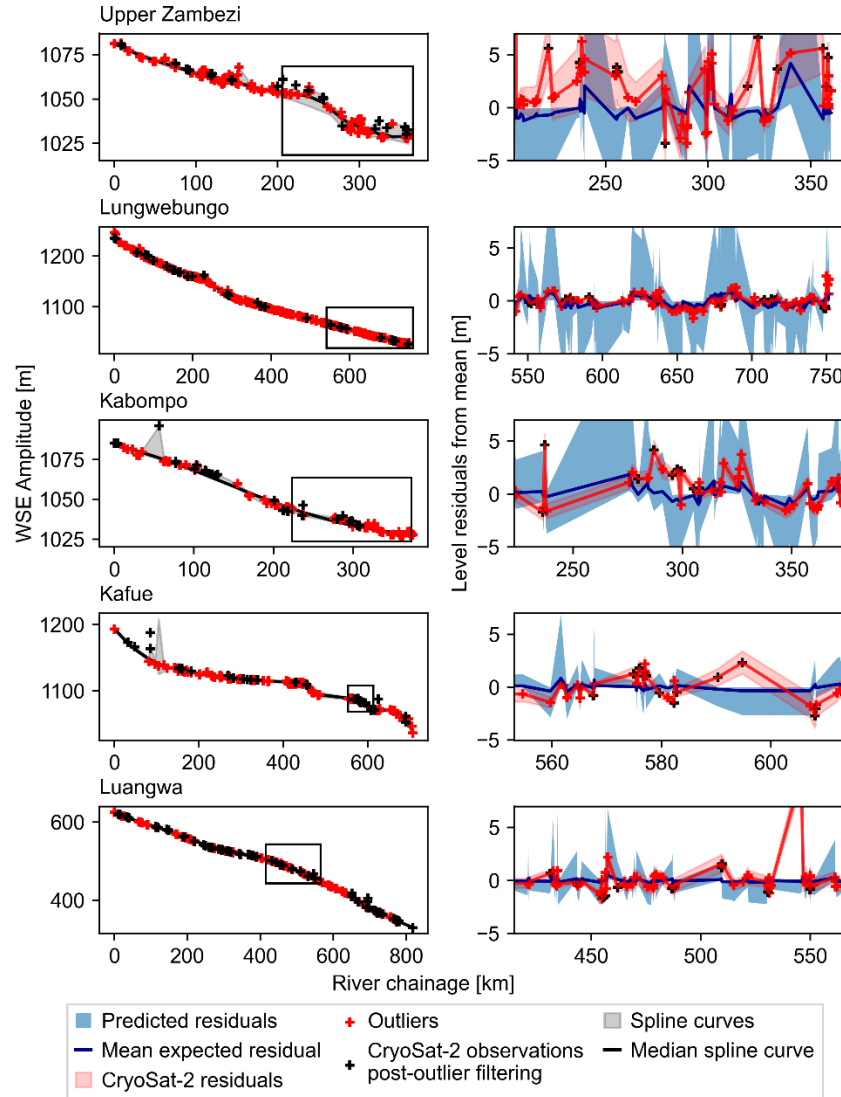


Figure 3 Selection of CryoSat-2 observations in the Zambezi. Left: longitudinal profile of each studied river reach, right: illustration of the outlier filtering process for a subset of each reach.

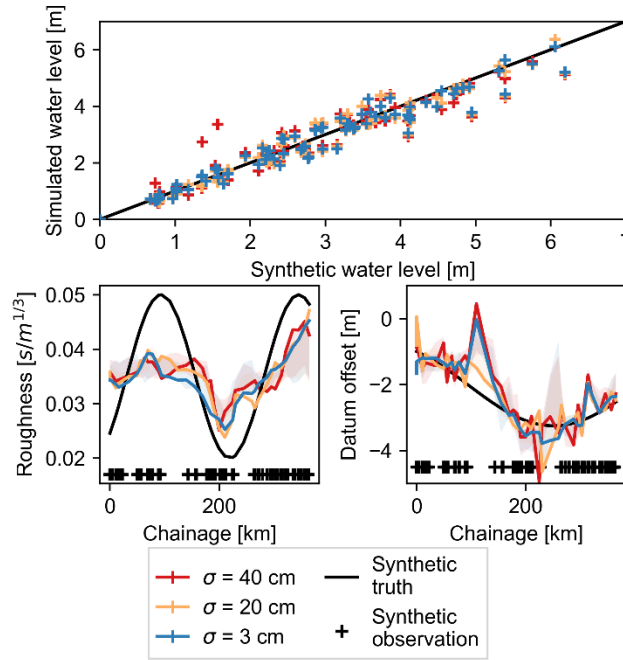
The main challenges in terms of outlier-filtering are adequately fitting the spline function so it is representative of the mean water surface profile along the river line. In the Upper Zambezi, Kafue and Kabompo we removed observations deviating from the spline function by more than twice the residual standard deviation and fitted a new spline function through the remaining observations, resulting in rejection rates of 18%, 19% and 23% respectively. This was necessary due to the combination of large variations in WSE and changes in the reach slope. There is a fine balance between overfitting outliers and smoothing the mean water level.

The Luangwa River runs from North-East to South-West. CryoSat-2 predominantly crosses the Luangwa between March and end of November, thus missing the wet season. Therefore, the CryoSat-2 observations are expected to be relatively close to the mean water elevation with very small predicted residuals. In this case the outlier filtering is particularly sensitive to the estimation of the mean water surface profile. However, reducing the smoothing factors of the spline curve ensemble also increased the risk of admitting clear outliers.

5.2. Synthetic test

The synthetic tests evaluate the impact of observation uncertainties by using respectively 3 cm, 20 cm and 40 cm standard deviations to perturb the synthetic CryoSat-2 observations. The results are shown in **Figure 4**.

350



351

352 **Figure 4** Top: Simulated against synthetic water level (the calibrated bed elevation is subtracted)
 353 for the three experiments. Bottom: Retrieval of synthetic Manning's roughness, n (left) and
 354 offset from the initial datum guess (right) by the model. The black crosses indicate the chainage
 355 of the synthetic observations consistent with the CryoSat-2 observation density.

356 A difference in performance is seen when increasing the observation uncertainty, as seen in the performance
 357 statistics (**Table 2**) and the spread in the scatter plot in **Figure 4**. The RMSD is in the order of magnitude of the
 358 observation uncertainty. For all assumed uncertainty levels, parameter retrieval is most improved at cross-sections
 359 with synthetic observations. This was expected and confirms the advantage of using spatially dense observations to
 360 calibrate hydrodynamic parameters. The weighted objective used in calibration includes a smoothness factor. There
 361 is good consistency between the RMSD and calibration objective, with the smoothness factor forcing a reduction in
 362 variations where the observation density is low.

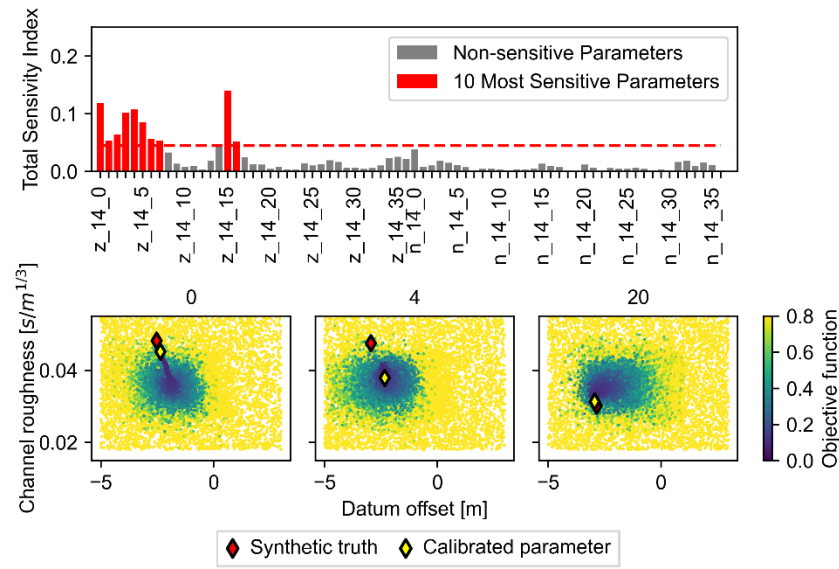
363 **Table 2** Calibration performance for the synthetic experiments at all cross-sections and at cross-
 364 sections with synthetic observations (gauged cross-sections).

Observation uncertainty	$\sigma = 40$ cm	$\sigma = 20$ cm	$\sigma = 3$ cm
WSE objective	0.26	0.15	0.09
RMSD [m]	0.33	0.17	0.08
Datum offset RMSD [m]	0.75	0.49	0.56
Considering only gauged cross-section	0.53	0.39	0.39
Manning's n RMSD [$s/m^{1/3}$]	0.0083	0.0072	0.0075

365

366 The downstream sections are most sensitive during calibration according to the FAST sensitivity analysis. The
 367 Saint-Venant equations account for backwater effects; therefore, changes in downstream parametrization have an
 368 impact on all upstream evaluation points. Tweaking upstream parameters will mainly impact the upstream
 369 predictions in the steady-state solver and thus have limited effect on the overall performance. Sensitivity is driven by
 370 the observation density, as seen for the parameters at cross-section 12, which correspond to the first large gap in
 371 observations, and are not sensitive at all (**Figure 4** and **Figure 5**).

372



373

374

375

376

377

378

Figure 5 Top: FAST sensitivity analysis of the synthetic calibration test with 20 cm standard deviation; the parameters are numbered from downstream to upstream cross-sections. Bottom: Sampling pattern and model performance during calibration at three randomly selected cross-sections. Cross-section numbering is from downstream to upstream. The objective is lowered during calibration.

379

380

381

382

383

384

385

The analysis also confirms that the objective function is less sensitive to the channel roughness, n , than the datum offset, z , as shown in **Figure 5** (top). The scatter plots in **Figure 5** provide information on whether trade-offs during calibration can explain the low sensitivity of the channel roughness. We plot the results of the low uncertainty calibration, to remove the effect of observation uncertainty on the parameter retrieval. During calibration, the parameters converge to relatively narrow parameter spaces. The synthetic truth is not always within the optimum range, which is due to the global objective function and trade-offs between parameters at the different cross-sections.

386

387

388

389

390

391

392

393

394

395

The bed elevation and channel roughness have similar local effects: overestimating the channel roughness raises the water level but can be compensated by slightly decreasing the bed elevation locally. Previous studies have shown that the two parameters impact the water surface differently over different characteristic spatial scales (Durand et al., 2014; Wood et al., 2016). When calibrating a single, global roughness parameter, the bed elevation will tend to have a local impact, whereas adjustments of the friction parameter will have a more diffuse effect and impact a longer portion of the reach. Thus, the two parameters can be retrieved simultaneously. In this study, both parameters are calibrated locally, and both have a local impact. This can be seen at cross-section 0, where the best performing parameter samples (objective function less than 0.2) form a straight line towards the synthetic truth. Thus, although parameters can be retrieved successfully at some cross-sections, there is still model ambiguity (e.g., at cross-section 4). The ambiguity can be partially resolved by increasing the observation density.

396

5.3. Calibration using real-world CryoSat-2 observations in the Zambezi

397

398

399

400

Figure 6 shows the calibrated longitudinal water surface profiles at the five locations in the Zambezi after calibrating the steady-state solver against real-world CryoSat-2 observations. Overall, the simulated WSE corresponds quite well to the CryoSat-2 observations.

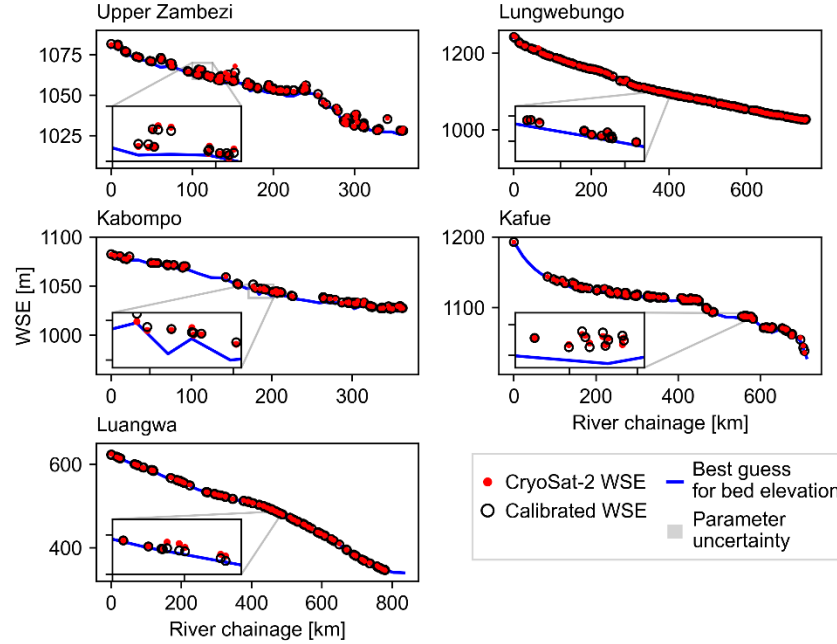


Figure 6 Calibrated longitudinal profile of the bed elevation and the WSE simulated by the steady-state solver for the five subreaches in the Zambezi – the calibrated WSE is computed using the discharge of the corresponding day of observation by CryoSat-2 assuming steady-state.

LISFLOOD-FP models are run for each reach using the calibrated channel roughness and bed elevation. **Table 3** summarizes performance statistics of the calibration and evaluation based on the steady-state solver and the transient solution respectively. We compare the simulated and observed water level by subtracting calibrated bed elevation from the satellite altimetry WSE. This removes the otherwise dominating effect of elevation on the performance. Overall performance is good and consistent across performance metrics. The weighted objective includes a smoothness and shallowness preference and is therefore generally larger than the RMSD. There is a good correlation between the simulated WSE and CryoSat-2 WSE. The RMSD is between 0.58 m and 0.88 m.

Figure 7 shows the WSE time series simulated by LISFLOOD-FP against the in-situ records at Chavuma and Watopa and against the Sentinel-3 WSE. We note that there are some timing issues in the water level prediction, particularly at Chavuma, and in the low flow predictions at Watopa. These are consistent with uncertainties in the rainfall-runoff model, which forces the steady-state hydraulic model and hydrodynamic models. Sentinel-3 is a SAR altimeter and expected to have a lower uncertainty than a conventional altimeter (3-30 cm in the Zambezi, according to Kittel et al., 2020b). We represent the Sentinel-3 data with a slightly higher uncertainty, as the stations used in this study could not all be evaluated against in-situ observations. A conservative upper bound of 50 cm, consistent with previous studies on altimetry observations of inland water (Villadsen et al., 2016) was therefore selected to indicate the Sentinel-3 uncertainty in **Figure 7**.

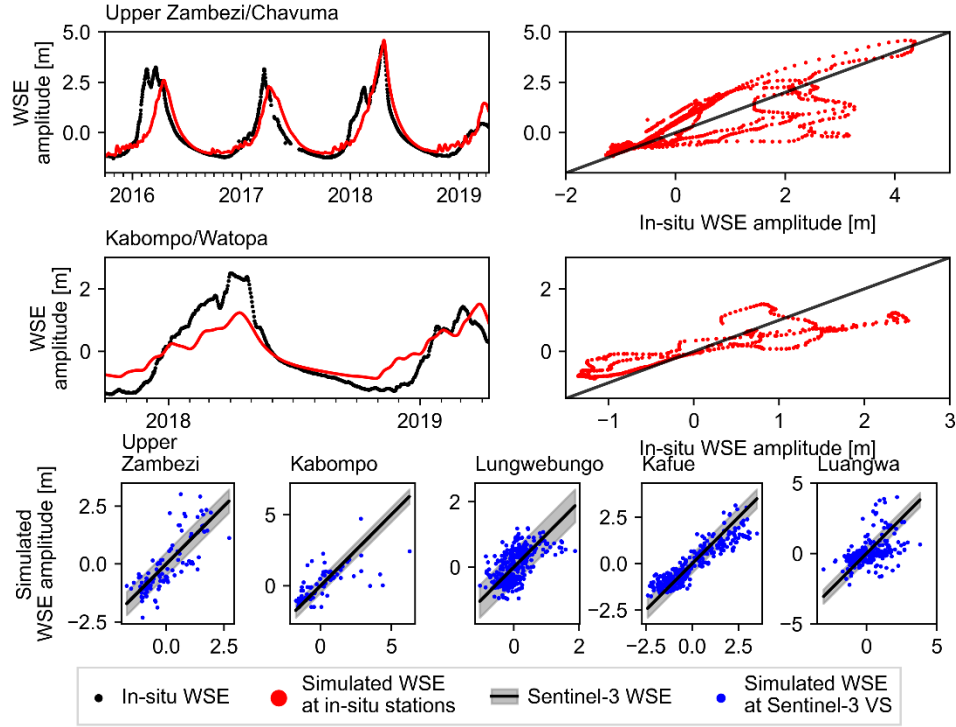


Figure 7 Dynamic WSE at in-situ stations Chavuma (Upper Zambezi – top row) and Watopa (Kabompo – middle row) and simulated by LISFLOOD-FP and Sentinel-3 WSE versus simulated WSE by LISFLOOD-FP at Sentinel-3 VS (bottom row). The shaded area represents the expected uncertainty of Sentinel-3 of up to 50 cm.

The steady-state and transient solutions differ by around 20 to 40 cm in RMSD against CryoSat-2 observations, which is in the order of magnitude of the expected CryoSat-2 uncertainty in LRM (Villadsen et al., 2016). The difference between the steady-state and transient solution (22 cm to 98 cm) can be partly explained by 1) the difference between the subgrid representation of the channel and the 1-dimensional line representation of the steady-state solver and 2) the coarser spatial resolution (900 m instead of 250 m) needed to allow reasonable computation time. The performance metrics remain comparable or better than results reported in previous studies.

Table 3 Steady-state (SS) solver and LISFLOOD-FP (L) performance statistics using calibrated parametrization and CryoSat-2 observations (C2), Sentinel-3 (S3) WSE and in-situ water level observations. The Pearson and Spearman correlation coefficients are calculated by subtracting the calibrated bed elevation from the CryoSat-2 observations to remove the effect of elevation on the performance. A p-value below 2.5% is considered significant – in all cases the p-value is below the threshold and the correlation is significant.

	Weighted objective	RMSD					Non-parametric KGE		Pearson r^2			Spearman r^2		
Data source	C2	C2	S3	In-situ	C2	In-situ	C2	In-situ	C2	S3	In-situ	C2	S3	In-situ
Solver	SS	SS vs. L	SS	L	L	L	L	L	L	L	L	L	L	L
Upper Zambezi	0.68	0.39	0.83	0.79	0.71	0.73	0.79	0.25	0.91	0.79	0.84	0.79	0.82	0.92
Lungwebungo	0.78	0.98	0.88	1.31	0.43		0.50		0.37	0.58		0.53	0.58	

Kabompo	0.45	0.32	0.61	0.71	1.14	0.60	0.89	0.49	0.90	0.69	0.90	0.90	0.79	0.90
Kafue	0.74	0.35	0.89	1.05	0.62		0.78		0.85	0.91		0.85	0.90	
Luangwa	0.54	0.17	0.66	0.60	0.99		0.11		0.58	0.43		0.44	0.61	

Overall, the performance is consistent with previous studies with RMSD values between 0.60 and 1.31 m. Jiang et al. (2019) obtained RMSD between the simulated and altimetry WSE between 0.72 m and 1.6 m, when using various combinations of altimetry datasets, with CryoSat-2 alone giving a calibration performance of 1.28 m. Domeneghetti et al. (2014) obtained a RMSD of around 1 m using Envisat data to calibrate a hydrodynamic model of the Po river. O'Loughlin et al. (2020) achieved RMSD between 0.84 and 2.02 m in the Congo when comparing a large-scale hydraulic model forced with in-situ and simulated discharge. As in this study, the channel depths and friction were calibrated against satellite altimetry WSE observations; however, the study used a global channel friction parameter.

6. Discussion

6.1. CryoSat-2 data selection

The CryoSat-2 observations used in the calibration must be accurate and representative of the river WSE. CryoSat-2 is not error-free and is difficult to validate due to the high spatial sampling but low temporal sampling frequency. In this study, we used hydrological simulations from a calibrated hydrological model to assess the validity of the CryoSat-2 observations. Instead of selecting a fixed threshold to assess the deviation of a given CryoSat-2 observation from the local river surface longitudinal profile, we predict the expected range of water level deviation based on the hydrological conditions in the reach at the time of observation.

Robust outlier removal is essential but highly challenging in poorly instrumented catchments. By exploiting simulations of discharge, which are already available as input to the hydraulic model, a more refined method was developed in this study. Valid observations may be rejected due to errors in the corresponding simulated discharge. This is likely to occur in poorly gauged catchments, where calibration is constrained by data availability. Retaining these observations may introduce errors in the calibration, as it fits the parameters to produce water levels, which are unlikely to have occurred under the simulated flow conditions. In this study, we demonstrate the method in a sparsely gauged catchment, where the added value of altimetry WSE is high. In future studies, we recommend applying this method in a highly instrumented catchment to validate the proposed method.

6.2. Model performance

The steady-state assumption of the solver is a simplification of the actual hydrodynamic conditions; it can be run for specific time steps corresponding to satellite overpasses greatly reducing computational time. The results are in the order of magnitude of the calibration data uncertainty and comparable to previous studies. This confirms that the method can be used to calibrate hydraulic models efficiently against spatially dense WSE observations.

Furthermore, simplifications are necessary to represent poorly instrumented river channels for hydraulic modelling. In particular, some assumption on the cross-section geometry is required (e.g., trapezoidal, rectangular channel, power channel). In this study, we select a simple rectangular shape, and use global river width databases to obtain the missing information about the mean width. An alternative approach could be to use a power-law to correlate the area and water depth and the conveyance and water depth, removing the need for an explicit definition of the channel shape.

Neal et al. (2015) investigated incorporating the channel cross-section uncertainty into large-scale flood inundation models of data sparse areas and showed that performance improved in models with calibrated channel friction and rectangular channels. Their results suggest that a channel shape parameter, roughness and elevation could be fitted simultaneously, provided sufficient dynamic observations are available in the reach. Neal et al. (2015) also showed that informing the model with even basic information about the channel geomorphology, such as width-discharge curves from optical or radar satellite imagery improved model calibration against level observations. The shape and friction have similar effects locally and calibrating the shape parameter may be more appropriate than calibrating friction for narrow channels, where the assumption of a rectangular shape is less appropriate.

The calibration of local variations in channel roughness greatly increases the parameter space, and poses a further challenge. Jiang et al. (2019) demonstrated that altimetry alone is insufficient to calibrate geometry parameters as well as a spatially distributed channel roughness. The reason for this is clear: local channel conveyance depends on both the channel roughness and flow area. Thus, there is model ambiguity and additional datasets are required to constrain the increased parameter space (e.g., channel width under known flow conditions). The unknown channel bed elevation prevents a satisfactory calibration of the level to area relationship and channel roughness. Thus, an interesting future path could include exploring whether the geometry parameters could be sufficiently constrained from alternative or new remote sensing observations, or whether calibrating local changes in channel geometry may be more robust than calibrating the channel roughness.

6.3. 1D versus 2D hydrodynamic model

The steady-state solver is one-dimensional and thus does not include bank overflow and floodplain processes. This will introduce errors in shallow reaches during extreme events, where the peak water level might be over-predicted to accommodate the high flow in a rectangular channel. Therefore, we only consider tributary branches of the Zambezi. The subgrid solver in LISFLOOD-FP calculates the floodplain water level when the level in the channel exceeds the bank elevation. This requires a robust match between bed and bank elevation. **Figure 8** illustrates the calibrated cross-sections versus the DEM at selected locations of the five reaches. Because the steady-state solver only calibrates the bed elevation, the bank elevation is extracted from the DEM. This poses a challenge if the calibrated bed is equal to or higher than the DEM elevation height, e.g., in the Upper Zambezi (**Figure 8**). The calibration information then becomes obsolete. If the difference is too small, the channel might overflow too often (as might be the case at Kabompo). Thus to apply the results in a 2D modelling setup, the bank elevation must be corrected, to ensure the channel is correctly burned into the floodplain, e.g. using SAR imagery to deduce the bank and bed elevation relationship (Wood et al., 2016). Despite the higher demands for parametrization and computation power, a two-dimensional solver would be necessary to adequately model the entire Zambezi, particularly the delta, which is not included in this study. The proposed method may however still be a useful steppingstone for more complex modelling efforts, particularly in poorly instrumented catchments.

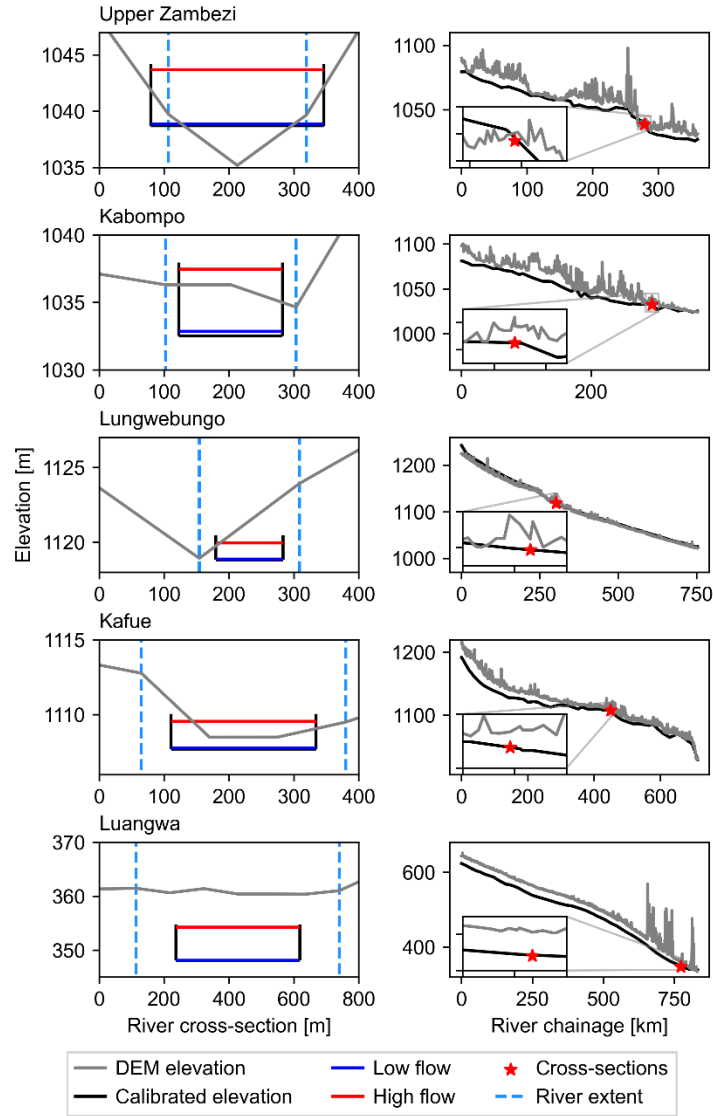


Figure 8 Selected calibrated river cross-sections versus MERIT DEM bed and bank elevations (left) and calibrated bed elevation versus the MERIT DEM river surface longitudinal profiles (right).

The DEM will usually give the elevation of the water surface in the channel at time of observation. This means that the calibrated bed elevation is more likely to be below than above the DEM elevation. The opposite occurs at Chavuma, where the slope is very high. CryoSat-2 observations before and after the drop in elevation force a compromise.

7. Conclusion

A reasonable hydraulic representation of river channels for large-scale flood modeling is essential but challenging to obtain in data poor regions. In this study, we propose using a steady-state solver to calibrate hydraulic parameters against geodetic altimetry observations. We propose an informed outlier rejection framework based on simulated discharge to select CryoSat-2 observations for calibration. The approach successfully removes obvious outliers, while allowing reasonably large deviations from the estimated mean level, provided there is coherence with the hydrological conditions on the day of observation. Furthermore, it ensures that only coherent forcing/observation

pairs are included in the calibration. The method enables filtering spatially dense WSE observations from geodetic satellite altimetry missions in data sparse regions, where traditional outlier identification methods fail. Hydraulic parameter retrieval was evaluated in synthetic experiments, focusing on the impacts of observation density and quality, and on the calibration setup. Bed elevation was retrieved with a RMSD of 42–75 cm and channel roughness with a RMSD of 0.007–0.009 s/m^{1/3}. The calibration revealed a higher sensitivity to the elevation offset compared to the roughness parameter, resulting in a poor retrieval of the upstream channel roughness. Furthermore, we noted the effect of the WSE observation density, with the most successful performance occurring in densely observed segments of the reach. Observation uncertainty affected the retrieval of parameters at ungauged cross-sections, and performance was more similar at gauged cross-sections for the three investigated data quality scenarios.

By carefully selecting observations where the steady-state assumption is reasonable, five reaches of the Zambezi were calibrated with satisfactory model performance using real CryoSat-2 observations. Calibration against real-world CryoSat-2 observations was evaluated using a range of statistical diagnostics to confirm the model behavior and compared to Sentinel-3 and in-situ observations of WSE to evaluate the temporal patterns of WSE in the river channels. The method yielded at least as good performance as past studies at far reduced computational cost and the parameter transfer from the steady-state to the transient solver did not impact performance significantly. Geodetic altimetry missions clearly hold valuable information for hydrological studies, particularly in ungauged basins. However, the dense spatial sampling requires careful data selection and comes at a computational cost because, in the hydraulic inversion, WSE must be simulated at all points of observation by the hydraulic forward model. The approach presented in this study integrates the altimetry observations in a fast and efficient, global calibration approach at low cost compared to a 1D hydrodynamic model.

References

- De Almeida, G. A. M., Bates, P., Freer, J. E., & Souvignet, M. (2012). Improving the stability of a simple formulation of the shallow water equations for 2-D flood modeling. *Water Resources Research*, 48(5), 1–14. <https://doi.org/10.1029/2011WR011570>
- Alsdorf, D. E., Rodríguez, E., & Lettenmaier, D. P. (2007). Measuring Surface Water From Space. *Reviews of Geophysics*, 45(2006), 1–24. <https://doi.org/10.1029/2006RG000197>.1.INTRODUCTION
- Berrisford, P., Dee, D. P., Poli, P., Brugge, R., Fielding, M., Fuentes, M., et al. (2011). The ERA-Interim archive Version 2.0, (1), 23. Retrieved from <https://www.ecmwf.int/node/8174>
- Biancamaria, S., Bates, P. D., Boone, A., & Mognard, N. M. (2009). Large-scale coupled hydrologic and hydraulic modelling of the Ob river in Siberia. *Journal of Hydrology*, 379(1–2), 136–150. <https://doi.org/10.1016/j.jhydrol.2009.09.054>
- Boergens, E., Buhl, S., Dettmering, D., Klüppelberg, C., & Seitz, F. (2017). Combination of multi-mission altimetry data along the Mekong River with spatio-temporal kriging. *Journal of Geodesy*, 91(5), 519–534. <https://doi.org/10.1007/s00190-016-0980-z>
- Boergens, E., Nielsen, K., Andersen, O. B., Dettmering, D., & Seitz, F. (2017). Water levels of the Mekong River Basin based on CryoSat-2 SAR data classification. *Hydrology and Earth System Sciences Discussions*, (June), 1–22. <https://doi.org/10.5194/hess-2017-217>
- Dinardo, S., Fenoglio-Marc, L., Buchhaupt, C., Becker, M., Scharroo, R., Joana Fernandes, M., & Benveniste, J. (2018). Coastal SAR and PLRM altimetry in German Bight and West Baltic Sea. *Advances in Space Research*, 62(6), 1371–1404. <https://doi.org/10.1016/j.asr.2017.12.018>
- Domeneghetti, A., Tarpanelli, A., Brocca, L., Barbetta, S., Moramarco, T., Castellarin, A., &

Brath, A. (2014). The use of remote sensing-derived water surface data for hydraulic model calibration. *Remote Sensing of Environment*, 149, 130–141.
<https://doi.org/10.1016/j.rse.2014.04.007>

Duan, Q., Sorooshian, S., & Gupta, V. (1992). Effective and Efficient Global Optimization for Conceptual Rainfall-Runoff Models. *Water Resources Research*, 28(4), 1015–1031.

Durand, M., Neal, J., Rodríguez, E., Andreadis, K. M., Smith, L. C., & Yoon, Y. (2014). Estimating reach-averaged discharge for the River Severn from measurements of river water surface elevation and slope. *Journal of Hydrology*, 511, 92–104.
<https://doi.org/10.1016/j.jhydrol.2013.12.050>

ESA. (2017). *Land Cover CCI Product User Guide Version 2. Tech. Rep.* Retrieved from maps.elie.ucl.ac.be/CCI/viewer/download/ESACCI-LC-Ph2-PUGv2_2.0.pdf

Frappart, F., Calmant, S., Cauhopé, M., Seyler, F., & Cazenave, A. (2006). Preliminary results of ENVISAT RA-2-derived water levels validation over the Amazon basin. *Remote Sensing of Environment*, 100(2), 252–264. <https://doi.org/10.1016/j.rse.2005.10.027>

Getirana, A. C. V., Boone, A., Yamazaki, D., & Mognard, N. (2013). Automatic parameterization of a flow routing scheme driven by radar altimetry data : Evaluation in the Amazon basin. *Water Resources Research*, 49(1), 614–629. <https://doi.org/10.1002/wrcr.20077>

Gupta, H. V., Kling, H., Yilmaz, K. K., & Martinez-Baquero, G. F. (2009). Decomposition of the Mean Squared Error & NSE Performance Criteria: Implications for Improving Hydrological Modelling. *Journal of Hydrology*, 377(1–2), 80–91.
<https://doi.org/10.1016/j.jhydrol.2009.08.003>

Hannah, D. M., Demuth, S., van Lanen, H. A. J., Looser, U., Prudhomme, C., Rees, G., et al. (2011). Large-scale river flow archives: Importance, current status and future needs. *Hydrological Processes*, 25(7), 1191–1200. <https://doi.org/10.1002/hyp.7794>

Houska, T., Kraft, P., Chamorro-Chavez, A., & Breuer, L. (2015). SPOTting model parameters using a ready-made python package. *PLoS ONE*, 10(12), 1–22.
<https://doi.org/10.1371/journal.pone.0145180>

Huffman, G., Bolvin, D., Braithwaite, D., Hsu, K., Joyce, R., & Xie, P. (2014). Integrated Multi-satellite Retrievals for GPM (IMERG), version 4.4. *NASA's Precipitation Processing Center*. Retrieved from <ftp://arthurhou.pps.eosdis.nasa.gov/gpmdata/>

Jiang, L., Nielsen, K., Andersen, O. B., & Bauer-Gottwein, P. (2017). CryoSat-2 radar altimetry for monitoring freshwater resources of China. *Remote Sensing of Environment*, 200(August), 125–139. <https://doi.org/10.1016/j.rse.2017.08.015>

Jiang, L., Madsen, H., & Bauer-Gottwein, P. (2019). Simultaneous calibration of multiple hydrodynamic model parameters using satellite altimetry observations of water surface elevation in the Songhua River. *Remote Sensing of Environment*, 225, 229–247.
<https://doi.org/10.1016/j.rse.2019.03.014>

Kittel, C. M. M., Nielsen, K., Tøttrup, C., & Bauer-Gottwein, P. (2018). Informing a hydrological model of the Ogooué with multi-mission remote sensing data. *Hydrology and Earth System Sciences*, 22, 1453–1472. <https://doi.org/10.5194/hess-22-1453-2018>

Kittel, C. M. M., Jiang, L., Tøttrup, C., & Bauer-Gottwein, P. (2021). Sentinel-3 radar altimetry

for river monitoring - A catchment-scale evaluation of satellite water surface elevation from Sentinel-3A and Sentinel-3B. *Hydrology and Earth System Sciences*, 25(1), 333–357. <https://doi.org/10.5194/hess-25-333-2021>

Liu, G., Schwartz, F. W., Tseng, K.-H., & Shum, C. K. (2015). Discharge and water-depth estimates for ungauged rivers: Combining hydrologic, hydraulic, and inverse modeling with stage and water-area measurements from satellites. *Water Resources Research*, 51, 6017–6035. <https://doi.org/10.1002/2015WR017200.A>

Mahé, G., Lienou, G., Descroix, L., Bamba, F., Paturel, J. E., Laraque, A., et al. (2013). The rivers of Africa: Witness of climate change and human impact on the environment. *Hydrological Processes*, 27(15), 2105–2114. <https://doi.org/10.1002/hyp.9813>

Maillard, P., Bercher, N., & Calmant, S. (2015). New processing approaches on the retrieval of water levels in Envisat and SARAL radar altimetry over rivers: A case study of the São Francisco River, Brazil. *Remote Sensing of Environment*, 156, 226–241. <https://doi.org/10.1016/j.rse.2014.09.027>

Michailovsky, C. I., & Bauer-Gottwein, P. (2014). Operational reservoir inflow forecasting with radar altimetry: the Zambezi case study. *Hydrol. Earth Syst. Sci.*, 18(3), 997–1007. <https://doi.org/10.5194/hess-18-997-2014>

Michailovsky, C. I., McEnnis, S., Berry, P. A. M. M., Smith, R., & Bauer-Gottwein, P. (2012). River monitoring from satellite radar altimetry in the Zambezi River basin. *Hydrology and Earth System Sciences*, 16(7), 2181–2192. <https://doi.org/10.5194/hess-16-2181-2012>

Myers, E., Hess, K., Yang, Z., Xu, J., Wong, A., Doyle, D., et al. (2007). VDatum and strategies for national coverage. *Oceans Conference Record (IEEE)*. <https://doi.org/10.1109/OCEANS.2007.4449348>

Neal, J., Schumann, G., & Bates, P. (2012). A subgrid channel model for simulating river hydraulics and floodplain inundation over large and data sparse areas. *Water Resources Research*, 48(W11506), 1–16. <https://doi.org/10.1029/2012WR012514>

Neal, J. C., Odoni, N. A., Trigg, M. A., Freer, J. E., Garcia-Pintado, J., Mason, D. C., et al. (2015). Efficient incorporation of channel cross-section geometry uncertainty into regional and global scale flood inundation models. *Journal of Hydrology*, 529, 169–183. <https://doi.org/10.1016/j.jhydrol.2015.07.026>

Nielsen, K., Stenseng, L., Andersen, O. B., Villadsen, H., & Knudsen, P. (2015). Validation of CryoSat-2 SAR mode based lake levels. *Remote Sensing of Environment*, 171, 162–170. <https://doi.org/10.1016/j.rse.2015.10.023>

O’Loughlin, F., Trigg, M. A., Schumann, G. J. P., & Bates, P. D. (2013). Hydraulic characterization of the middle reach of the Congo River. *Water Resources Research*, 49(8), 5059–5070. <https://doi.org/10.1002/wrcr.20398>

O’Loughlin, F. E., Neal, J., Schumann, G. J. P., Beighley, E., & Bates, P. D. (2020). A LISFLOOD-FP hydraulic model of the middle reach of the Congo. *Journal of Hydrology*, 580(September 2019), 124203. <https://doi.org/10.1016/j.jhydrol.2019.124203>

Paiva, R. C. D., Collischonn, W., Bonnet, M. P., De Gonçalves, L. G. G., Calmant, S., Getirana, A., & Santos Da Silva, J. (2013). Assimilating in situ and radar altimetry data into a large-

scale hydrologic-hydrodynamic model for streamflow forecast in the Amazon. *Hydrology and Earth System Sciences*, 17, 2929–2946. <https://doi.org/10.5194/hess-17-2929-2013>

Paris, A., Dias de Paiva, R., Santos Da Silva, J., Medeiros Moreira, D., Calmant, S., Garambois, P.-A., et al. (2016). Stage-discharge rating curves based on satellite altimetry and modeled discharge in the Amazon basin. *Water Resources Research*, 53, 3787–3814.

<https://doi.org/10.1002/2014WR016618>. Received

Pekel, J.-F., Cottam, A., Gorelick, N., & Belward, A. S. (2016). High-resolution mapping of global surface water and its long-term changes. *Nature*, 540(7633), 418–422.

<https://doi.org/10.1038/nature20584>

Pool, S., Vis, M., & Seibert, J. (2018). Evaluating model performance: towards a non-parametric variant of the Kling-Gupta efficiency. *Hydrological Sciences Journal*, 63(13–14), 1941–1953. <https://doi.org/10.1080/02626667.2018.1552002>

Saltelli, A., Tarantola, S., & Chan, K. P. (1999). A Quantitative Model-Independent Method for Global Sensitivity Analysis of Model Output A Quantitative Model-Independent Method for Global Sensitivity Analysis of Model Output. *Technometrics*, 41(1), 39–56.

Schneider, R., Godiksen, P. N., Villadsen, H., Madsen, H., & Bauer-Gottwein, P. (2017). Application of CryoSat-2 altimetry data for river analysis and modelling. *Hydrology and Earth System Sciences*, 21, 751–764. <https://doi.org/10.5194/hess-21-751-2017>

Schneider, R., Ridler, M. E., Godiksen, P. N., Madsen, H., & Bauer-Gottwein, P. (2018). A data assimilation system combining CryoSat-2 data and hydrodynamic river models. *Journal of Hydrology*, 557, 197–210. <https://doi.org/10.1016/j.jhydrol.2017.11.052>

Schneider, R., Tarpanelli, A., Nielsen, K., Madsen, H., & Bauer-Gottwein, P. (2018). Evaluation of multi-mode CryoSat-2 altimetry data over the Po River against in situ data and a hydrodynamic model. *Advances in Water Resources*, 112, 17–26.

<https://doi.org/10.1016/j.advwatres.2017.11.027>

Schumann, G., Di Baldassarre, G., Alsdorf, D., & Bates, P. D. (2010). Near real-time flood wave approximation on large rivers from space: Application to the River Po, Italy. *Water Resources Research*, 46(5), 1–8. <https://doi.org/10.1029/2008WR007672>

Schwatke, C., Dettmering, D., Bosch, W., & Seitz, F. (2015). DAHITI - An innovative approach for estimating water level time series over inland waters using multi-mission satellite altimetry. *Hydrology and Earth System Sciences*, 19(10), 4345–4364.

<https://doi.org/10.5194/hess-19-4345-2015>

Sosa, J., Sampson, C., Smith, A., Neal, J., & Bates, P. (2020). A toolbox to quickly prepare flood inundation models for LISFLOOD-FP simulations. *Environmental Modelling and Software*, 123(October 2019), 104561. <https://doi.org/10.1016/j.envsoft.2019.104561>

Tarboton, D. (2015). TauDEM Version 5. *Hydrology Research Group, Utah State University*. Retrieved from <http://hydrology.usu.edu/taudem/taudem5/documentation.html>

Tourian, M. J., Tarpanelli, A., Elmi, O., Qin, T., Brocca, L., Moramarco, T., & Sneeuw, N. (2016). Spatiotemporal densification of water level time series by multimission satellite altimetry. *Water Resources Research*, 52, 613–615.

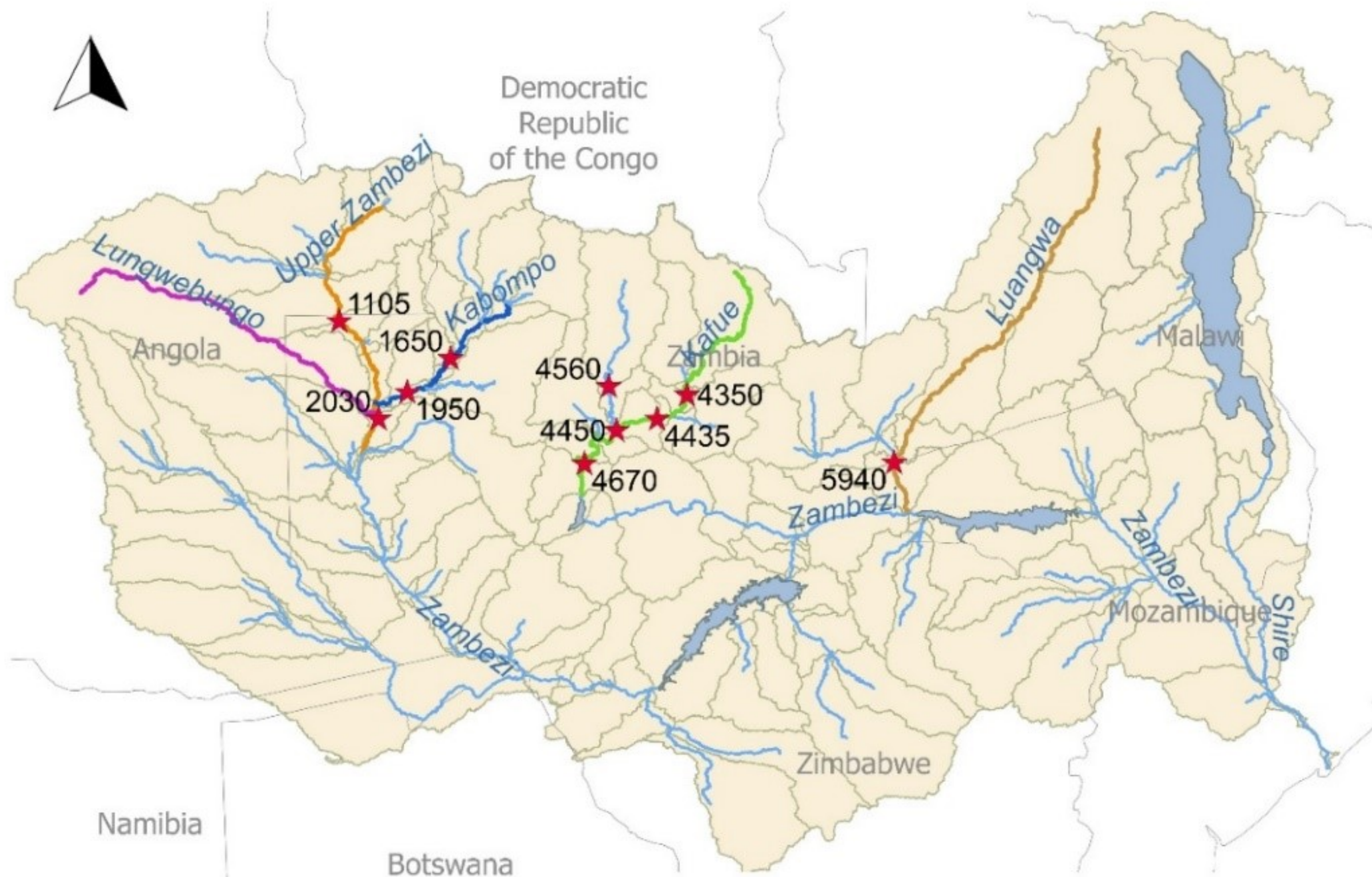
<https://doi.org/10.1029/2008WR006912>.M

- Villadsen, H., Deng, X., Andersen, O. B., Stenseng, L., Nielsen, K., & Knudsen, P. (2016). Improved inland water levels from SAR altimetry using novel empirical and physical retrackers. *Journal of Hydrology*, 537, 234–247. <https://doi.org/10.1016/j.jhydrol.2016.03.051>
- Vörösmarty, C., Askew, A., Grabs, W., Barry, R. G., Birkett, C., Döll, P., et al. (2001). Global water data: A newly endangered species. *Eos*, 82(5), 54–58. <https://doi.org/10.1029/01EO00031>
- Westerberg, I. K., Guerrero, J. L., Younger, P. M., Beven, K. J., Seibert, J., Halldin, S., et al. (2011). Calibration of hydrological models using flow-duration curves. *Hydrology and Earth System Sciences*, 15(7), 2205–2227. <https://doi.org/10.5194/hess-15-2205-2011>
- Wood, M., Hostache, R., Neal, J., Wagener, T., Giustarini, L., Chini, M., et al. (2016). Calibration of channel depth and friction parameters in the LISFLOOD-FP hydraulic model using medium-resolution SAR data and identifiability techniques. *Hydrology and Earth System Sciences*, 20(12), 4983–4997. <https://doi.org/10.5194/hess-20-4983-2016>
- Zhang, L., Potter, N., Hickel, K., Zhang, Y., & Shao, Q. (2008). Water balance modeling over variable time scales based on the Budyko framework - Model development and testing. *Journal of Hydrology*, 360, 117–131. <https://doi.org/10.1016/j.jhydrol.2008.07.021>
- Zhang, X., Jiang, L., Kittel, C. M. M., & Yao, Z. (2020). On the performance of Sentinel-3 altimetry over new reservoirs : Approaches to determine on-board a-priori elevation. *Geophysical Research Letters*, 47(17), 1–11. <https://doi.org/10.1029/2020GL088770>

Acknowledgments, Samples and Data

The authors wish to thank the Zambezi River Authority (ZRA) for kindly providing the in-situ observations in the Upper Zambezi used to evaluate the WSE simulations. The data can requested from the ZRA for research purposes. The Sentinel-3 data used in this study can be freely processed on and downloaded from the ESA GPOD (Grid Processing on Demand SAR Versatile Altimetric Toolkit for Ocean Research and Exploitation) service (available on <https://gpod.eo.esa.int/>, last accessed 14/10/2020). The MERIT DEM used as reference elevation and in the river delineation was obtained from http://hydro.iis.u-tokyo.ac.jp/~yamada/MERIT_DEM/, last accessed 14/10/2020). The rainfall-runoff model source code is open source and part of the GlobWetland Africa QGIS Toolbox (available on <http://globwetland-africa.org/?wpdmpo=globwetland-toolbox-1-5>, last accessed 17/11/2020). LISFLOOD-FP can be requested on <http://www.bristol.ac.uk/geography/research/hydrology/models/lisflood/downloads/> (last accessed 17/11/2020). The CryoSat-2 observations and model parameters will be made available on Zenodo and are provided as supplement to this article.

Figure 1.



Legend

★ In-situ gauging stations Subbasins River line

Figure 2.

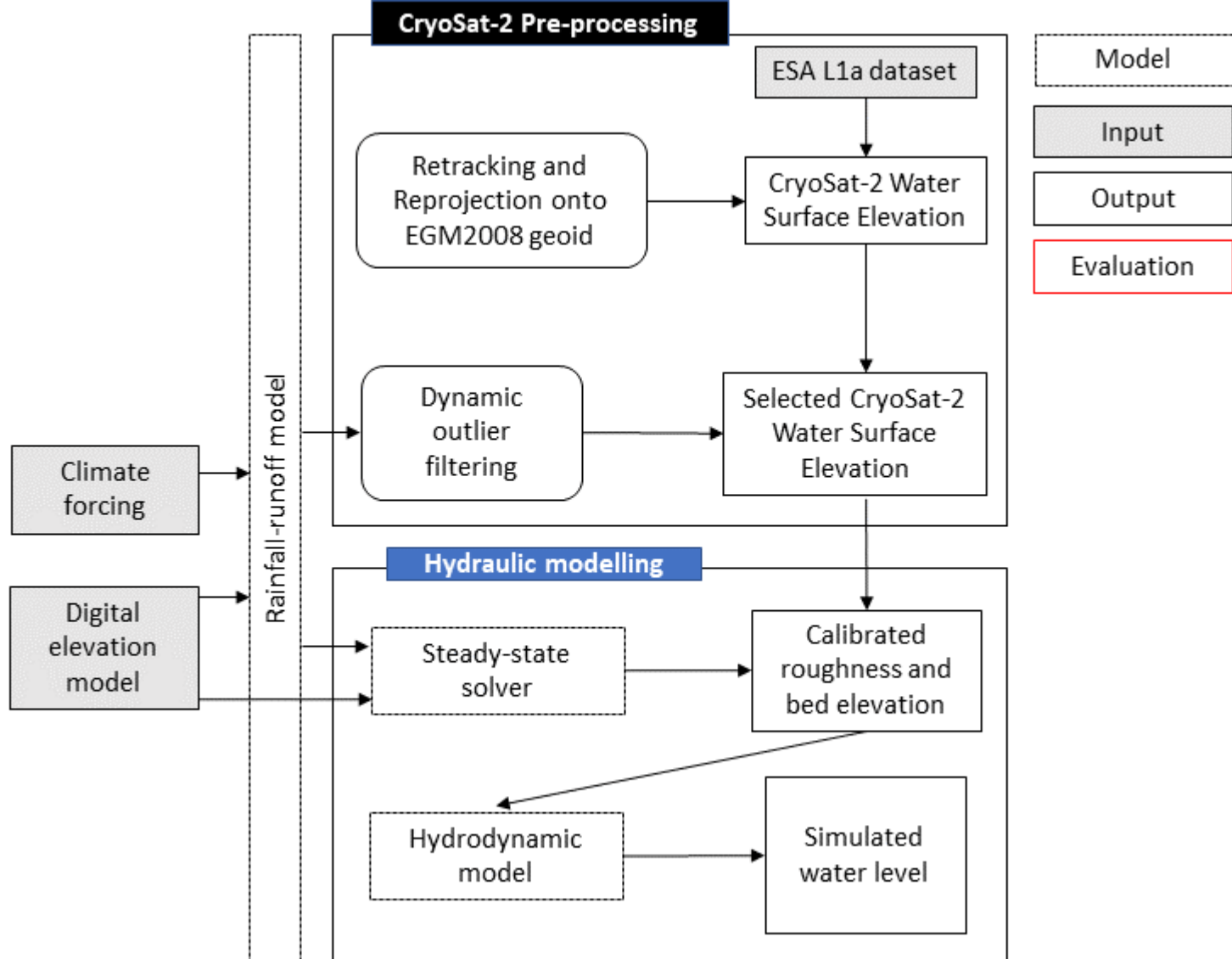


Figure 3.

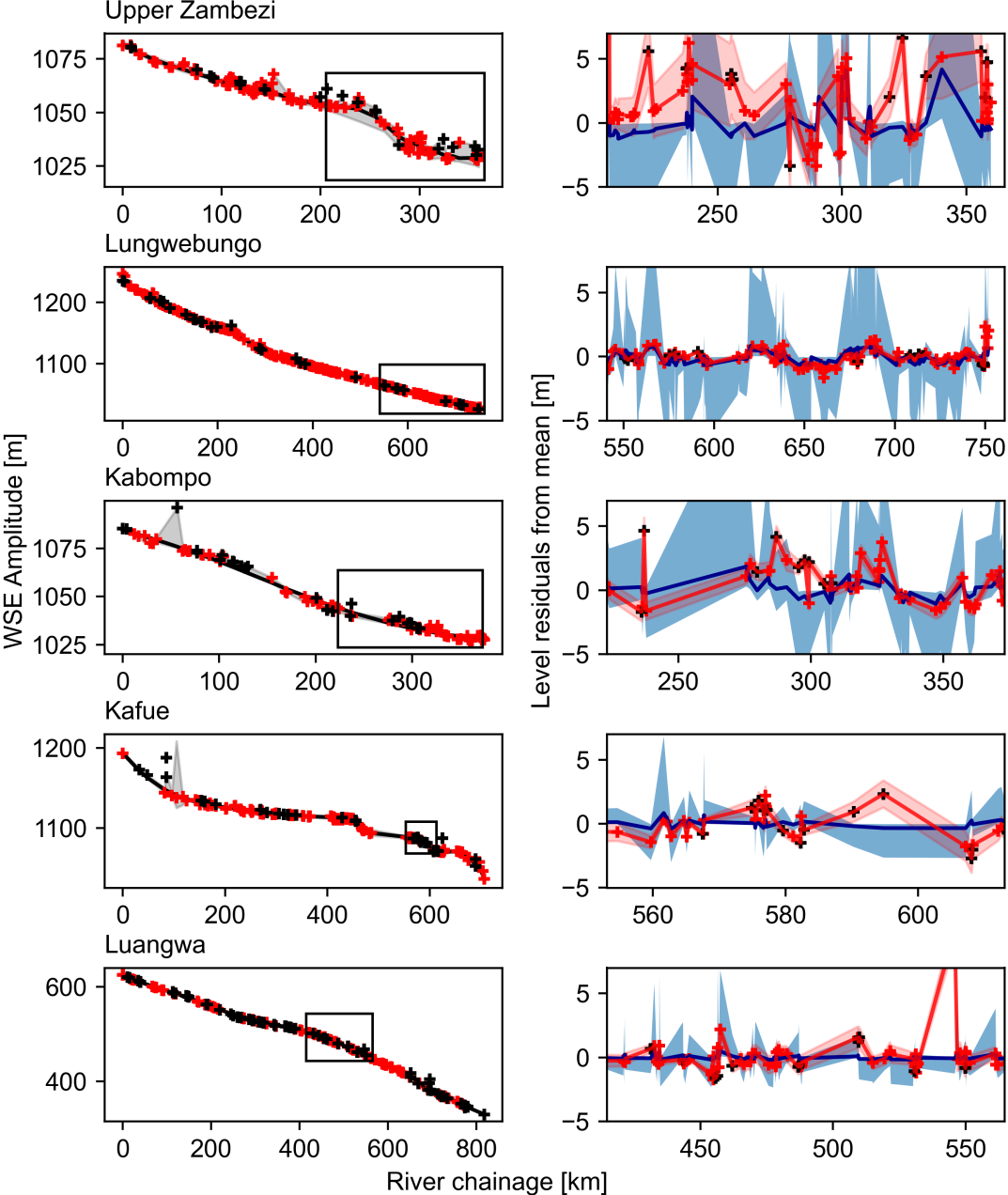


Figure 4.

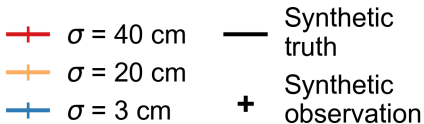
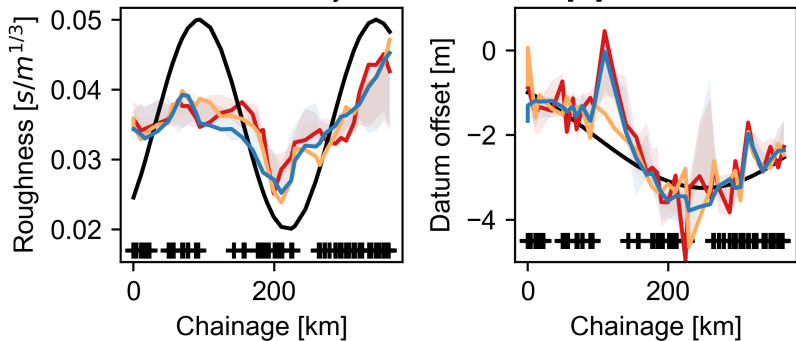
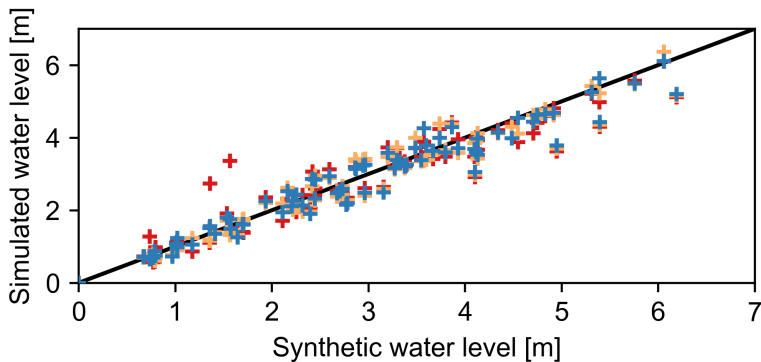


Figure 5.

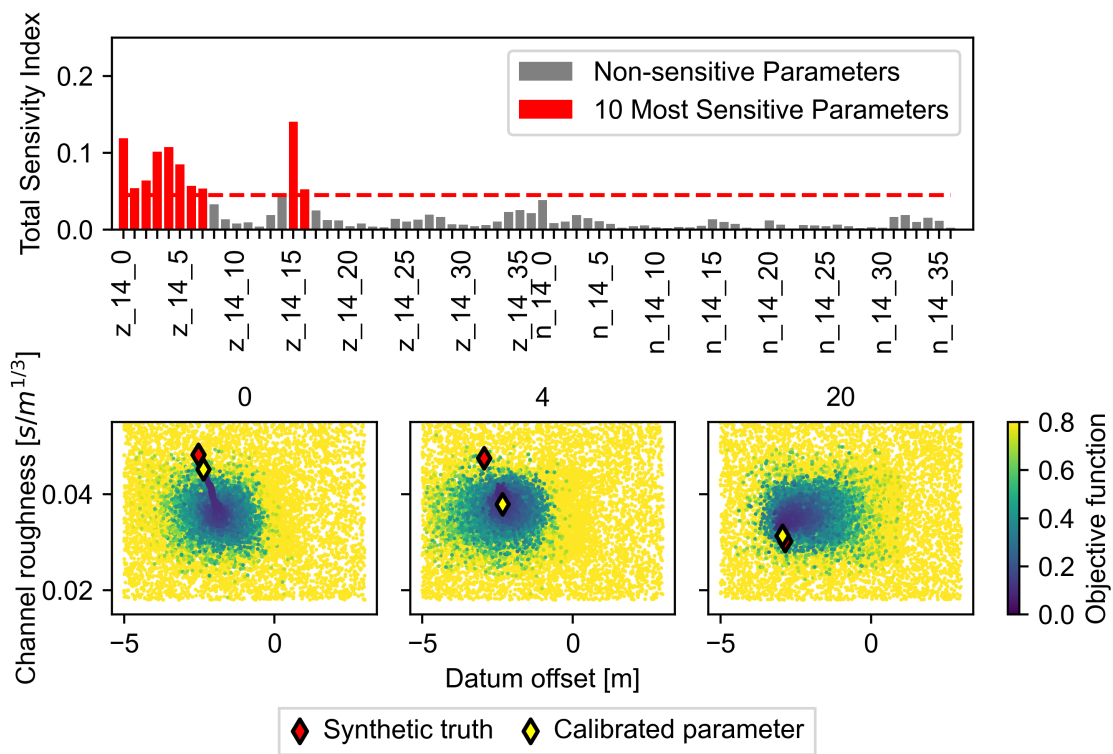
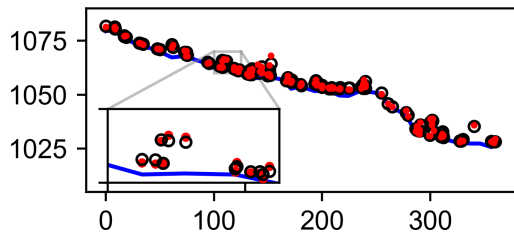
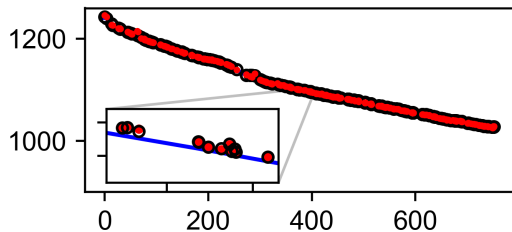


Figure 6.

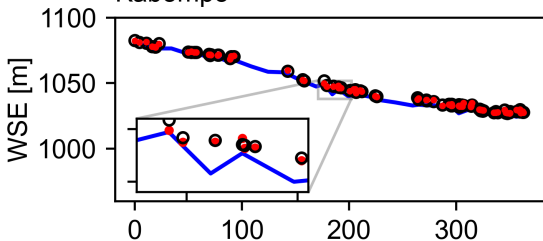
Upper Zambezi



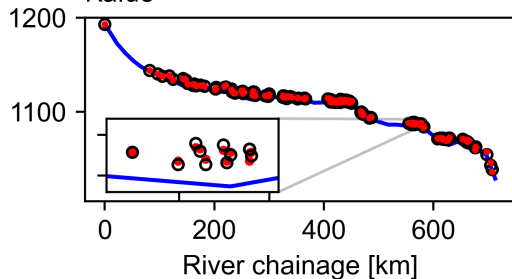
Lungwebungo



Kabompo



Kafue



Luangwa

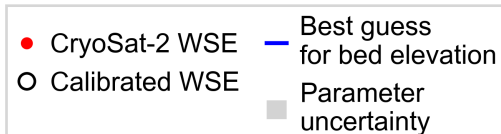
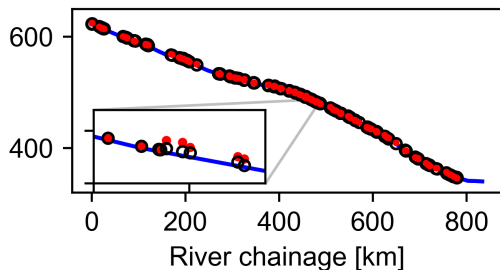
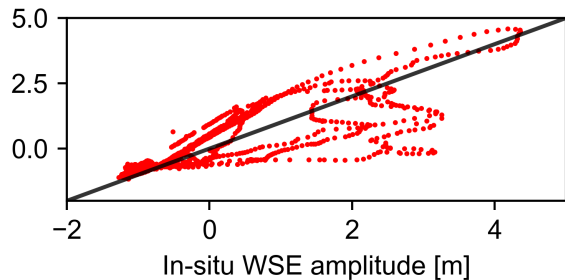
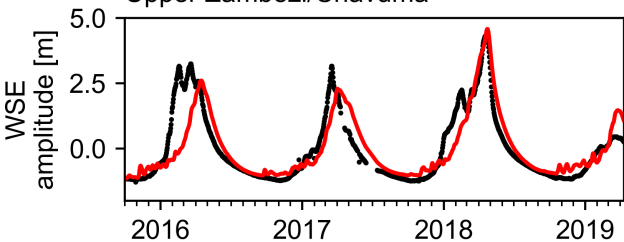


Figure 7.

Upper Zambezi/Chavuma



Kabompo/Watopa

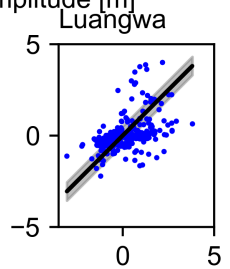
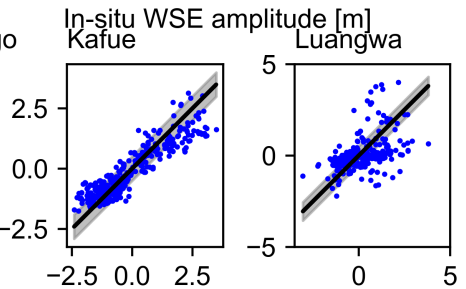
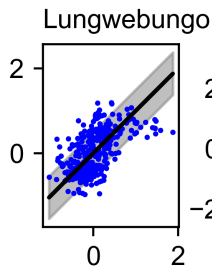
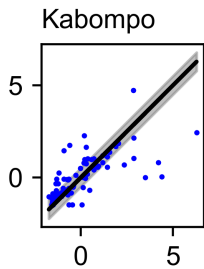
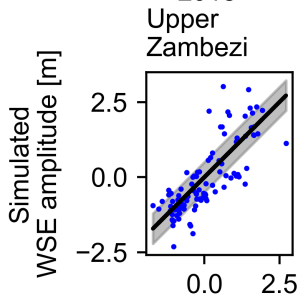
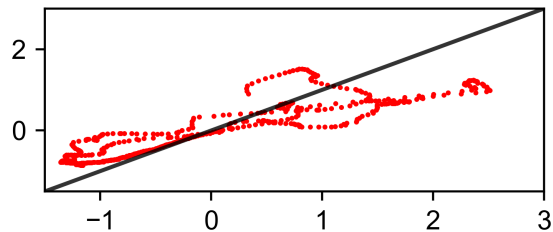
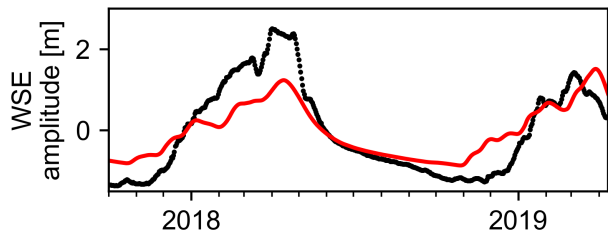


Figure A1.

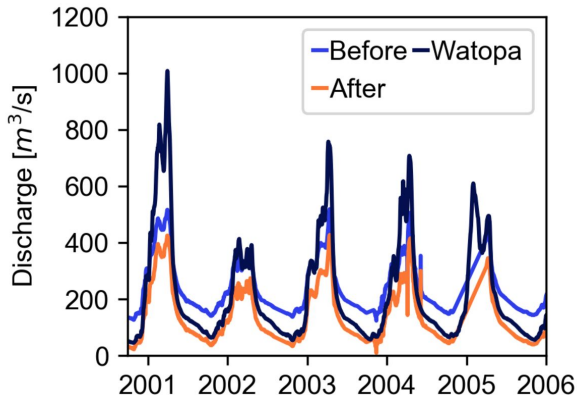
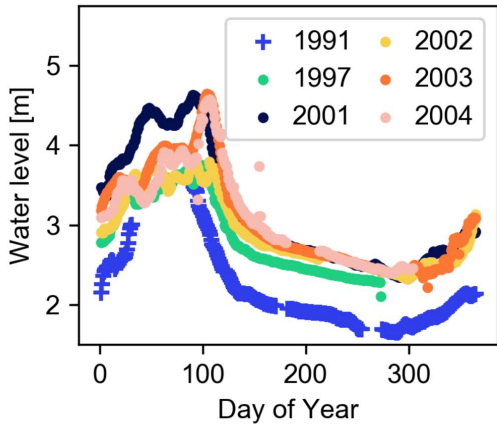


Figure 8.

